Self-Attention AI Model for Practical Sensor Networking: Demodulation of Long-Period Fiber Grating Sensor Cascaded with FBG Sensor Array

Felipe Oliveira Barino, *Member, IEEE,* and Alexandre Bessa dos Santos, *Member, IEEE*

***Abstract*— This paper proposes a cost-effective solution for interrogating long-period fiber grating (LPFG) sensors using an optical fiber sensor network. The network comprises an array of fiber Bragg grating (FBG) sensors, whose reflection spectrum are modulated by the LPFG's transmission spectrum. A self-attention AI model decodes these spectral modulations to extract the LPFG's resonant wavelength. The AI model dynamically filters the FBG reflection spectra, focusing on the most relevant features for LPFG demodulation. It is trained using synthetic data and validated with measured LPFG spectra. The system achieves sub-nanometric demodulation resolution (0.75 nm RMSE and 0.0335% MAPE) for a set of 73 LPFG spectra. In a practical application using a refractive index LPFG sensor, the system demonstrates a relative error of less than 1%. This approach, combining an FBG array with a synthetically trained self-attention AI model, offers a promising pathway towards more practical and cost-effective LPFG interrogation in multi-sensor networks.**

***Index Terms*— fiber optic sensors, Bragg gratings, interrogation, neural networks, self-attention, sensor network**

I. INTRODUCTION

FIBER Bragg gratings (FBGs) and long-period fiber gratings (LPFGs) are well-established technologies in optical fiber sensing, offering high sensitivity for diverse applications. While FBG interrogation possesses well-defined techniques and readily available commercial solutions, extracting meaningful data from LPFGs remains a significant hurdle for in-field applications. This discrepancy stems from the fundamental differences in their spectra: FBGs exhibit a sharp, well-defined reflection peak, whereas LPFGs possess a broader, more complex transmission spectrum. This complex interrogation paradigm holds back the widespread adoption of LPFGs as practical sensors [1].

One key challenge lies in the need for broadband spectral measurements to extract features relevant to LPFG calibration. For instance, an LPFG's resonant dip can span tenths of nanometers, necessitating the measurement of broad spectrum for detecting its resonant wavelength. Consequently, current LPFG interrogation often relies on bulky and/or expensive equipment, often to interpret a single sensor.

The spectral width of LPFGs also presents significant limitations for quasi-distributed sensing. Notably, FBGs can be easily multiplexed in the wavelength domain, allowing numerous sensing points to be monitored simultaneously using the same cable and optoelectronics, significantly reducing system cost-effectiveness [2], [3]. Conversely, the broader bandwidth limits the number of multiplexed LPFGs to fewer devices [4], [5].

However, LPFG sensor technology holds immense promise. LPFGs offer a simpler fabrication process compared to FBGs, employing direct-write techniques like point-by-point electric arc discharge [6], [7], [8], point-by-point laser irradiation [9], [10], [11] or laser scanning [12], [13]. Additionally, dynamic LPFGs induced by mechanical deformations present interesting possibilities for sensing applications [14], [15].

Beyond their ease of fabrication, LPFGs possess broader measurand capabilities than FBGs. Their inherent sensitivity to refractive index is applied to a wide range of sensing applications [16], [17]. LPFG-based sensors have found success in diverse fields. An example is the food industry with olive oil deterioration [18] and coffee fermentation [19]. Its use as biosensing platform is also quite promising, with label-free sensors for DNA sequence detection [20], detection of vitamin D [21], bacterial detection [22], pepsin detection [23], hemoglobin quantification [24], and glucose quantification [25]. And, for structural health monitoring, with sensors focused on humidity [26] and corrosion [27], [28], for example. This versatility highlights LPFGs as a promising platform for a vast array of measurands and fields. Therefore, developing cost-effective methods for interrogating and integrating these sensors holds the key to unlocking their widespread adoption beyond research labs.

II. LPG INTERROGATION STATE-OF-THE-ART

To address the interrogation challenge, researchers have proposed solutions to reduce interrogation system costs through sparse or dense filtering of the optical spectrum, aiming to capture features crucial for LPFG interrogation. Arrayed waveguide gratings (AWGs) offer a potential approach for estimating the entire spectrum, in [29], [30] the authors showed the curve-fitted LPFG spectrum can be used to estimate the resonant wavelength with 0.07 nm to 1 pm when considering a thermally tunable AWG. However, such approach uses a photodiode array, to reduce the photodiode count, authors have

This work was supported in part by the Coordenação de Aperfeiçoamento Pessoal de Nível Superior (CAPES), Conselho Nacional de Desenvolvimento Científico e Tecnológico (CNPq), Fundação de Amparo à Pesquisa do Estado de Minas Gerais (FAPEMIG), Instituto Nacional de Energia Elétrica (INERGE-UFJF), and Santo Antônio Energia.

F. O. B arino and A. B. dos Santos are with the Departmento de Circuitos, Universidade Federal de Juiz de Fora (UFJF), Juiz de Fora, Brazil (e-mail: felipe.barino@ufjf.br, felipe.barino@ieee.org, alexandre.bessa@ufjf.br).

Color versions of one or more of the figures in this article are available online at http://ieeexplore.ieee.org

proposed the use of modulated light sources. In [31] the resonant wavelength was detected using temperature modulated lasers in the range of 1530 to 1570 nm with 1.12 nm shift from real and in [32] a multimode laser, also thermally modulated, could estimate the LPFG's resonance with 0.4 nm accuracy. However, the thermal system is slow, and the final acquisition rate was 15 and 50 min, respectively. A more robust approach was presented in [33] , where a Fabry-Perot filter was applied to interrogate temperature, refractive index, and humidity with 4.9%. 2.75%, and 6.67% error at a reasonable acquisition rate (100 Hz). Sparse filters, leveraging the distinct reflection wavelengths of FBGs, have also been explored as filtering elements for LPFG demodulation [34], [35]. However, in those cases, the use of dual or even single edge filtering FBGs for LPFG interrogation imposes limits regarding LPFG spectral characteristics.

While the use of FBGs is interesting because of the natural know-how of researchers and engineers working in the field of optical fiber sensing, sparse filtering presents a complex challenge due to the intricate relationship between the filtered power and the LPFG spectrum. This task becomes particularly difficult without prior knowledge of the LPFG characteristics, as information loss can be significant. For example, edge filter interrogators need to be calibrated for individual LPFG transfer characteristics. Hence, by changing the LPFG sensor, the interrogator must be recalibrated. This limitation is detrimental to field use due to impracticability caused by LPFG width and depth changing. Note that LPFG's coupling efficiency might change as it shifts, especially for refractive index measurements, which is the main interest of this sensing technology. Adding more FBGs would improve generalization, but data processing and calibration complexity increases.

However, machine learning models have shown promising results for spectral reconstruction [36] and LPFG demodulation based on static FBG filters. Indeed, an array of 13 equally spaced FBGs was used to acquire spectral features of any given LPFG and those processed by machine learning algorithms to retrieve the LPFG resonant wavelength [37], [38]. A simple 3 layer and 5 hidden neuron multilayer perceptron was used to estimate an arbitrary LPFG resonance with 1.00 nm mean absolute error (MAE) [37] and this metric was enhanced to 0.668 nm by using better pre-processing strategy and further improved to 0.352 nm by using a fuzzy system for data processing [38].

The assumption of static FBGs, on the other hand, imposes some challenges. First, as the devices could fluctuate due to temperature changes, for example. This would introduce errors in the system, as the FBGs' position were encoded within the model during its training. Second, one optical circulator and photodetection circuit is needed per channel. Moreover, the most compelling advantage of using an FBG array for LPFG demodulation lies in its multi-sensing capability, which was yet to be explored [37], [38]

However, by introducing arbitrary FBGs (i.e., FBGs as sensing elements), we can enhance system cost-effectiveness while incorporating multi-point sensing capabilities. This allows FBGs to be used for strain and temperature sensing, while the LPFG serves various measurands not accessible by FBGs. Furthermore, a combination of two FBGs can compensate for the LPFG's cross-sensitivity to strain and temperature. This enables a quasi-distributed sensing system using the FBG array in a wavelength division multiplexing quasi-distributed architecture [39] alongside the intensity-modulated LPFG sensor. In this way, commercially available FBG interrogators could be adapted to acquire the reflection spectra of the FBG array with the reflection intensity modulated by the LPFG sensor.

The combined use of FBG and LPFG has been reported in the literature for simultaneous measurement of temperature and humidity [40], blood viscosity, glycated hemoglobin concentration, and micro-strain in vascular interventions [41], and temperature/pressure in pipeline structural health monitoring [42], thus providing LPFG compensation through FBG measurements. In these examples, transmission spectrum was considered, which makes the LPFG demodulation direct. However, by using only the reflection spectrum, LPFG-modulated intensity enables the use of simpler cable management and field-proven FBG interrogators.

Moreover, the use of arbitrary FBGs (where FBGs are sensors) and their reflection as a sparse and reconfigurable light source for LPFG illumination has not been reported and is the basis of this study, in which a novel solution to address this interrogation challenge is presented. Hence, we employ a cascaded configuration, comprising an LPFG sensor followed by an FBG sensor array containing 13 elements, creating a sensor network. We used a commercially available FBG interrogator to evaluate the position of all 14 sensors based on the captured reflection spectrum. While Bragg wavelengths detection is direct, and the sensing application is widely reported, the LPFG detection in this case is challenging. Hence, to demodulate the LPFG's position from the intensity modulation induced on the FBG reflections, we introduce a novel self-attention artificial intelligence model. The model extracts features from the FBG reflection and dynamically filters the most relevant for the given LPFG, hence only these are used to estimate the resonant wavelength.

The use of self-attention in optical fiber sensing signal processing has been adopted for Fabry-Perot strain sensor [43] and Mach-Zehnder interferometric displacement sensor [44]. And it is a promising solution for demodulation of the intensity-modulated LPFG-FBG sensor array. However, training such models often necessitates substantial amounts of data. To address this, we utilize synthetic data for model training and subsequent validation with real-world data. We posit that this approach of transfer learning from synthetic data can significantly accelerate the adoption of machine learning and artificial intelligence for sensor demodulation, as shown in [45]. By avoiding the time-consuming task of acquiring a large and meaningful dataset for complex model training, this methodology holds immense potential to pave the way for wider integration of AI-powered sensor interrogation techniques [45]. Additionally, the use of synthetic training allows for a more meaningful and comprehensive test/evaluation dataset, improving model's error characterization and, thus, reliability.

The innovation of this research lies in FBG-LPFG sensor networking and the solution for the intricate relationship between FBG reflection and LPFG position. To solve this

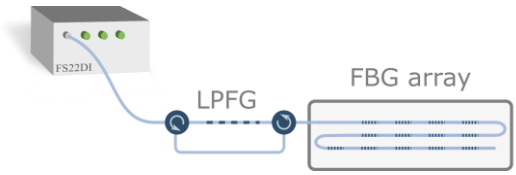

Fig. 1. Schematic of the optical setup considered in this work.

interaction and demodulate the LPFG position, we introduce a self-attention model for dynamic feature filtering and LPFG demodulation. Hence, this model enables the development of a novel and versatile sensor network configuration. Notably, the LPFG demodulation using an arbitrary FBG sensor array—without prior knowledge of LPFG transmissivity—and relying solely on the FBG array reflectivity profile modulated by the LPFG's dip has not been documented in existing literature. Furthermore, the proposed model was entirely developed using synthetic LPFG spectrum data, and the practical results were exceptional, paving the way for robust and well-characterized machine learning models for optical sensing, as experimental data could be utilized to further investigate error and reliability. One can access this paper code, model, data, and other supplementary material in [46].

III. Methods

A. Optical setup and spectral preprocessing

This work utilizes a straightforward optical configuration for sensor interrogation. The LPFG sensor and FBG sensor array were cascaded in series. So, in addition to the LPFG, the setup incorporates thirteen FBGs with center wavelengths ranging from approximately 1510 nm to 1590 nm. A commercially available FS22DI BraggMeter from HBM serves as the interrogation unit. The LPFG sensor was connected to the FS22DI output, followed by the FBG array.

Here, it's important to note that the initial setup would cause the light source from the interrogator to traverse the LPFG sensor twice – once before reaching the FBGs and again after reflection. This double pass would introduce significant optical attenuation. To mitigate this issue, we implemented a pair of optical circulators. These circulators ensure that only the light reflected by the FBG array interacts with the LPFG sensor. A schematic representation of the complete optical setup is provided in Fig. 1.

Using this FBG array we expect to demodulate LPFGs from 1515 nm to 1585 nm. Note that changes in the FBG array distribution, such as variations in FBG spacing, might impact the LPFG demodulation capability. However, the system could be tailored to specific FBG arrays, as the proposed model was developed to be transparent to FBG positioning. Overlapping is also a concern regarding FBG sensing, however, it could be solved using reported methods [49], [50], [51], [52] before preprocessing so the correct FBG peaks are detected.

The reflection spectrum measured by the FS22DI was processed to extract each of the Bragg wavelength and reflected intensity using a gaussian approximation of each reflection peak. This data array (2x13) was preprocessed in four steps and then fed to the machine learning model:

1) **Baseline Removal:** the raw peak intensities were first subtracted from a baseline measurement obtained without the LPFG present. This step compensates for variations in individual FBG reflectivity.
2) **Normalized Input Strength:** following baseline removal, the resulting peaks were divided by their total intensity, as described. This normalization yields an "input strength" array ranging from 0 to 1, with each value representing the relative contribution of a specific FBG to the overall reflection. This essentially indicates how close each FBG sensor is to the LPFG sensor.
3) **Normalized Bragg Wavelength:** a copy of the Bragg wavelength array (extracted from the reflection peaks) is created and normalized between 0 and 1. The normalization uses the minimum and maximum possible operating wavelengths (e.g., 1500 nm and 1600 nm).
4) **Feature Concatenation:** Finally, the normalized Bragg wavelength array is merged with the initial data array (containing normalized input strength).

This process results in a combined feature matrix of dimensions 3x13, where each row represents:

a) **Input Strength:** relative contribution of an FBG to the LPFG demodulation (0 to 1).
b) **Normalized Bragg Wavelength:** normalized value between 0 and 1 based on the operating wavelength range.
c) **Absolute Bragg Wavelength:** actual measured Bragg wavelength in nanometers.

This preprocessed data matrix serves as the input for the machine learning model, providing a comprehensive representation of the sensor array response for LPFG demodulation.

Fig. 2 summarizes all preprocessing steps, with the FBG reflection in solid red and the LPFG representation in dotted blue. The point plot shows the preprocessed data: the input strength. This proposal is interrogator-agnostic, meaning it can be used with any FBG interrogation unit capable of retrieving FBG wavelengths and reflection intensities.

B. Machine learning model

This work employs a self-attention-based fully connected neural network to demodulate the LPFG's resonant wavelength. The core concept behind this model is to achieve independence from the specific FBG positions within the array. This aligns with the "input strength" feature, which represents the relative

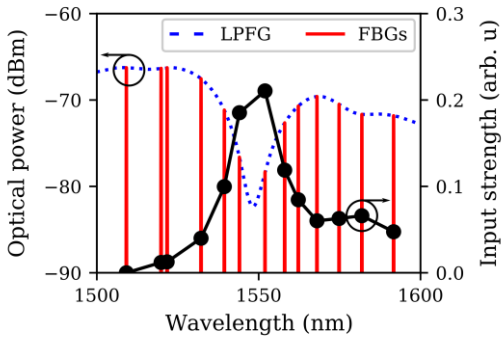

Fig. 2. Illustration of the preprocessing.

proximity of the LPFG to each FBG sensor. Ideally, an inner product of the input strength vector and the Bragg wavelength vector would directly yield the LPFG position.

However, the raw input strength alone lacks information about absolute FBG positions or the LPFG spectrum itself. To address this limitation, the self-attention model aims to refine the input data by generating a "filtered input strength" vector. This filtered vector, when used for an inner product with the Bragg wavelengths, should accurately estimate the LPFG position.

Hence, the model was thought of as a deep filter that generates the "filtered input strength". To do so, the input data is mapped to a higher dimensional space and processed to generate this vector. To exclude the effect of FBGs sensors far from the LPFG dip we employed self-attention to keep only the most relevant features.

The model architecture utilizes two hidden layers, named "hidden 1" and "hidden features," to extract informative features from the preprocessed data and represent them in the higher-dimensional space. It's important to note that not all extracted features might be relevant for a given LPFG demodulation. This could include noise, spectral power fluctuations, or even resonant dips outside the measurement range (potentially near the first or last FBGs).

To filter out these undesired elements, the model employs an attention mechanism. Attention mechanisms have proven valuable for sequential problems and demonstrate strong capabilities for complex data abstraction [47], [48]. In this context, the attention map is generated in a similar manner as the hidden features, but with a softmax activation function applied. This attention map serves to modulate the hidden features through point-wise multiplication. Note that attention's crucial aspect is the dynamic nature of the attention map. Unlike a pre-defined filter, the attention map is generated on-the-fly for each input data point. This dynamic characteristic allows the model to adaptively focus on the most relevant features based on the input data, leading to a more robust and generalizable filtering process for LPFG demodulation.

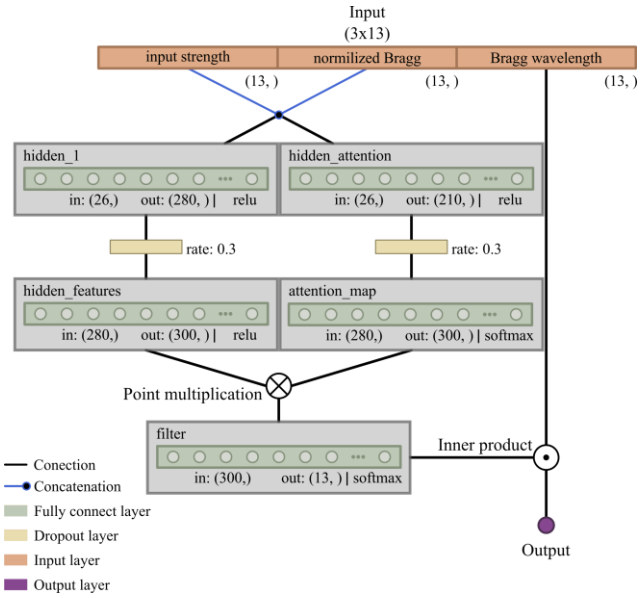

Fig. 3. Self-attention dense neural network.

Finally, the model generates a 13-element output vector. When this vector is used for an inner product with the Bragg wavelength vector, it should accurately estimate the LPFG position. A schematic representation of the complete model architecture is provided in Fig. 3.

The hyperparameters: layer size, activation, and dropout rate were all optimized by 200 trials of Bayesian optimization in the search space: layer sizes from 100 to 300 (discretized in tenths), dropout from 0.1 to 0.3 (discretized in 0.1), and activation function chosen between ReLU, tanh, and sigmoid.

The model was trained by Adam optimization with 0.001 learning rate. The model was fitted to the target resonant wavelength and to the filter output. The target filter output was calculated considering the relative distance between each FBG and the LPFG so that the inner product with the Bragg wavelength vector yields the target LPFG's resonant wavelength.

C. Training on synthetic data

The proposed self-attention model should achieve accurate LPFG demodulation but necessitates a substantial training dataset. This dataset must be reliable, sufficiently large, and diverse to encompass a wide range of LPFG characteristics and FBG sensor array configurations. Acquiring such a dataset solely through real-world measurements can be time-consuming and resource-intensive.

Fortunately, the characteristic shape of an LPFG spectrum can be effectively modeled using mathematical functions like modified Gaussian and Lorentzian functions. Leveraging this principle, we simulated synthetic LPFG spectra with diverse parameters. These parameters included:

- **Coupling efficiency**: the LPFG attenuation intensity;
- **Resonant wavelength:** the central wavelength of the LPFG's dip in the transmission spectrum;
- **Spectral Width:** the sharpness of the LPFG's spectral dip;
- **Secondary dips:** to mimic the presence of real-world spectral ripples, we incorporated additional dips within the simulated spectra;
- **Out-of-Range dips:** we also included resonant dips situated outside the FBG sensor array's wavelength range to further enhance the model's generalization capabilities by simulating potential real-world scenarios.

The FBG simulation followed a similar approach, with random Bragg wavelengths. Hence, a total of 400,000 samples

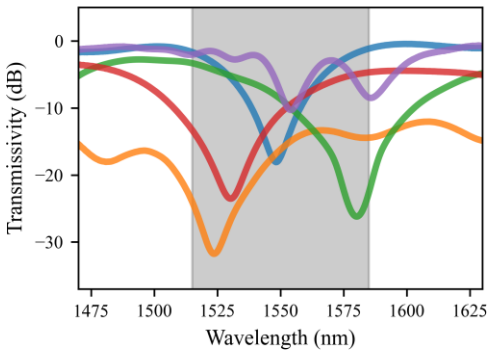

Fig. 4. Five samples of measured LPFG spectra.

were generated to perform model selection and another 1,000,000 new data were generated to fine tune the selected model. All the synthetic LPFG spectra considered in this work were randomly generated using uniform probability distribution function: dip depth $\in [10, 40]$ dB, $\lambda_{res} \in [1515, 1585]$ nm, FWHM $\in [15, 40]$ nm, and insertion loss $\in [0, 10]$ dB. The FBGs' Bragg wavelengths were also shifted considering a uniform distribution up to half the array spacing to avoid overlapping. Overlapping, as discussed, could be solved before preprocessing. The FBG FWHM was constant at 200 pm for all synthetic data, note, however, the FWHM should not impact on data processing as only the reflected peak was considered.

D. Model evaluation

We evaluated the proposed model using 73 LPFG transmission characteristics, measured by an OSA (Anritsu MS9740B). For each LPFG we considered 100 different FBG configurations, 7300 test data samples in total. Five measured LPFG transmission can be seen in Fig. 4, note the spectral variability (position, width and distortion). The shaded area represents the proposed technique target range.

The proposed model was compared to a robust fitting method to adjust the FBGs reflection to a Lorentzian function. This method is referred to as 'robust' because we employed several parameter restrictions, informed by the FBG array characteristics, to optimize the fitting process. We considered the metrics: R^2, root mean squared error (RMSE), mean absolute percentage error (MAPE).

Furthermore, we show an application example, using an LPFG refractive index (RI) sensor, the sensor was calibrated using the OSA and further interrogated by the proposed system. Note that FBGs are intrinsically capable of measuring strain and temperature, so presenting a RI LPFG sensor is coherent with the multi-point sensing scheme of our proposal. Moreover, the change in surrounding RI changes the LPFG's coupling efficiency, so it is a great opportunity to evaluate the interrogation capability when both the resonant wavelength and attenuation changes.

The FBGs' Bragg wavelengths were estimated as (OSA at 0.03 nm resolution bandwidth and 20001 sampling points from 1500 to 1600 nm): 1510.005, 1515.530, 1521.245, 1529.905, 1538.610, 1544.1, 1549.91, 1555.595, 1561.275, 1572.765, 1578.560, 1587.090, and 1590.160 nm and the FWHM of all devices was 0.226 ± 0.003 nm.

To assess the model's capability in managing FBG fluctuations, strain ramps were applied to three FBGs located near the LPFG's resonant dip while the LPFG sensor was submerged in water. The three FBGs closer to the LPFG resonant dip were shifted up to 800 pm using the deformation setup reported in [49].

IV. RESULTS

A. Exploring the attention mechanism

This section explores the behavior of the self-attention mechanism within the proposed model. We evaluated its performance in a controlled environment using synthetic data. The objective was to analyze how the hidden feature maps and the attention map adapt to the scenarios illustrated in Fig. 5. They are LPFG shifting, LPFG distortion, and FBG shifting:

1) **LPFG shifting:** We investigated how the model responds to changes in the LPFG's position within the sensor array.
2) **Distorted LPFG spectrum:** We evaluated the model's ability to handle distortions in the LPFG spectrum, potentially caused by environmental factors.
3) **FBG shifting:** We assessed the model's robustness to shifts in the FBG sensor array position.

The results reveal insightful observations. When the LPFG's resonant wavelength (central dip) shifts, the attention map exhibits significant changes. This indicates that the model effectively focuses on the relevant features within the hidden features based on the LPFG's spectral position. Interestingly, the hidden feature maps themselves show minimal variation in this scenario.

Conversely, for the same resonant wavelength but with a distorted spectrum (introduced ripples or additional dips), the attention map exhibits only minor modifications. This suggests that the model can effectively filter out these spectral distortions, focusing on the core features crucial for LPFG demodulation.

When the FBG sensor array is shifted, the attention map displays a slight spread. However, the core features of interest remain prominent. This demonstrates the model's ability to adapt to minor variations in the FBG array position while maintaining accurate LPFG demodulation.

Additionally, we conducted experiments varying only the LPFG width, coupling efficiency or resonant wavelength while all other parameters were randomly generated with uniform distribution. We found that all layers' output were only sensitive to the resonant wavelength, indicating that they indeed encode the LPFG center. The results can be found in this paper repository [46]. The dip's width and depth insensitivities show that the model is suitable for any LPFG sensor, including polarization-dependent sensors under multiple states of polarization, whereas dip broadening can happen significantly.

B. Results on measured LPFG spectra

The analysis of the attention mechanism using synthetic data provided valuable insights into its filtering behavior for LPFG demodulation. However, the true test of the model's effectiveness lies in its ability to deal with real-world scenarios. In this section, we leverage the high-resolution capabilities of an OSA to characterize actual LPFG spectra. By feeding these real-world spectra into the self-attention model for LPFG demodulation, we aim to validate the efficacy of the proposed approach that utilizes synthetic data training with transfer learning.

This evaluation is crucial for demonstrating the potential of our method. It allows us to assess how well the model, trained on synthetic data, can handle the complexities and imperfections present in actual LPFG measurements. Here, the real LPFG spectra might contain noise, spectral variations not captured perfectly by the simulations, and potential deviations from the ideal conditions assumed during synthetic data generation. Evaluating the model's performance with these real-world challenges will solidify the promise of synthetic training and transfer learning for LPFG demodulation using FBG sensor arrays.

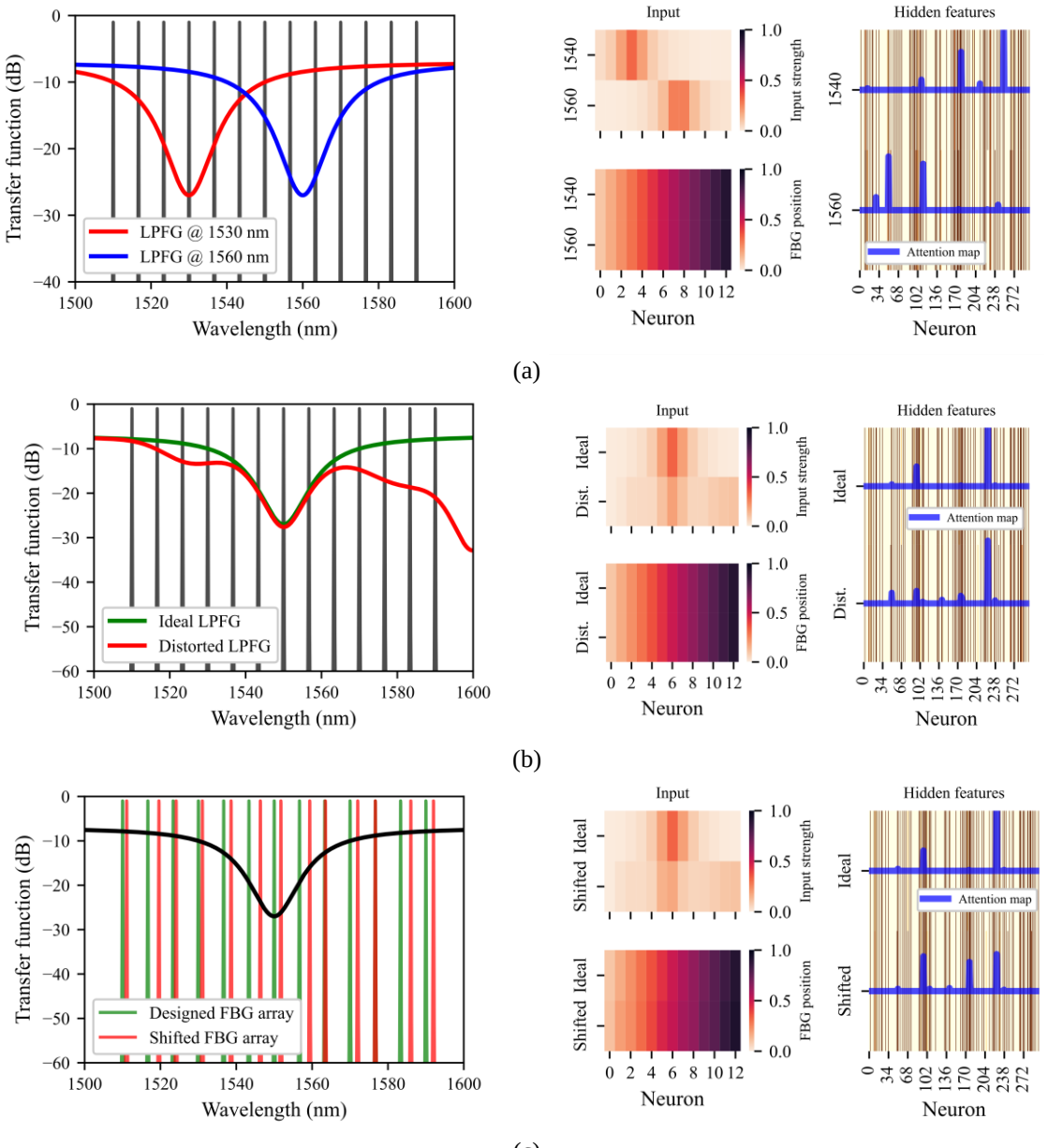

Fig. 5. Evaluating the attention mechanism regarding (a) shifted LPFG, (b) distorted LPFG, and (c) FBG shift.

In this evaluation, we tested 73 LPFG spectra from various arc-induced sensors. Each spectrum was evaluated using 100 FBG array configurations to comprehensively assess the model's generalizability. To quantify model uncertainty, we used the dropout layer to generate an ensemble of outputs and estimate the resonant wavelength and its uncertainty [50], [51], [52]. Additionally, each data point was processed using a Lorentzian fit, and uncertainty was estimated based on the fitted parameter's covariance matrix. Fig. 6 compares the performance of our proposed model with the baseline Lorentzian fitting approach.

Our findings demonstrated that the baseline model performs well for relatively simple spectra. However, for sensors with an additional resonant dip falling outside the FBG array's range (but potentially detectable by some FBGs), the baseline model's estimation suffers (evident in the outliers near 1555 nm). This is likely due to the high variability of actual LPFGs compared to the ideal Lorentzian function, leading to high parameter uncertainty in these cases.

The proposed model with the attention mechanism addresses these limitations. The attention layer effectively filters out irrelevant features, including those associated with resonant dips outside the FBG array range. This targeted filtering significantly improves the model's accuracy compared to the baseline approach.

Table I summarizes the performance metrics calculated using the measured LPFG spectra. We compared the models using the entire dataset and a subset excluding poorly fitted spectra by the Lorentzian model. In all aspects, the proposed model outperforms the baseline model, for both the complete and filtered datasets, we performed a t-test for the metrics, which indicated a statistically significant difference between the

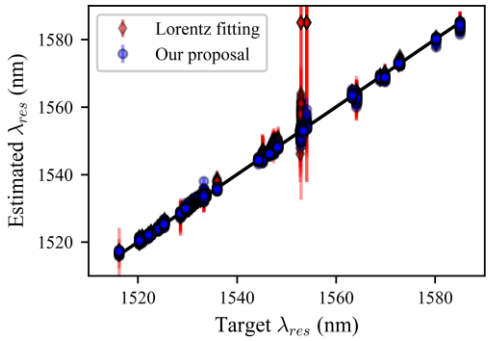

Fig. 6. Target vs estimated LPFG position.

means. These results are comparable to previous findings for neural networks trained with real LPFG data and static FBGs. This reinforces the effectiveness of both the FBG sensor interrogation technique for LPFG sensors and the proposed transfer learning approach using synthetic data.

Note that the curve fitting approach is a standard technique for LPFG-agnostic demodulation using a set of optical filters and presents a good resolution over limited range and closely spaced channels [29], [30], [32], [33]. However, the results for sparse filters, as presented in this paper, are not ideal. The proposed model, on the other hand, demonstrably outperforms the baseline Lorentzian fitting approach, achieving a reduction in RMSE from 2.13 nm to 0.75 nm for the complete dataset. Hence, the proposed method improves the state-of-the-art multi-channel-based LPFG demodulation for sparse filtering channels with moving filters (FBG sensors).

We estimated the system's resolution by the residues standard deviation and obtained a 0.687 nm resolution. Which was in line with the results found for neural networks presented in [38], [39] using static FBGs and trained with measured data. This indicates that the higher dimensional features coupled to the attention mechanism were able to filter the input data and correct the FBG shifts considered in this work, this also shows that the synthetic training was successful and derived similar results to measured-data training.

Overall, the evaluation using real LPFG spectra validates the effectiveness of synthetic data training with transfer learning for LPFG demodulation. Indeed, the results on measured data provide great insights on the generalization capabilities of the model. This approach offers a promising solution for practical

TABLE I. PERFORMANCE METRICS

		R^2	RMSE (nm)	MAPE (%)
Proposed model	*All data*	0.9977 ± 0.0002	0.75 ± 0.02	0.0335 ± 0.0001
	Without outliers	0.9980 ± 0.0001	0.70 ± 0.02	0.0321 ± 0.0001
Loretnzian fitted model	*All data*	0.982 ± 0.006	2.13 ± 0.35	0.050 ± 0.002
	Without outliers	0.9973 ± 0.0003	0.83 ± 0.04	0.039 ± 0.002

scenarios in which acquiring a large dataset of real-world LPFG measurements might be time-consuming or resource-intensive.

C. Practical demonstration

The LPFG sensor used for the practical application was a ~1540 nm arc-induced micro-tapered grating with 53 nm FWHM, 4.33 dB insertion loss, and 15.5 dB attenuation dip, in air. We applied different concentrations of water/glycerol mixtures from 10% to 50%, mixtures' RI was measured with an Abbe refractometer. Sensor calibration was conducted considering the shift from the water sample, to reduce temperature and strain cross-sensitivity.

Fig. 7 shows the calibration curve (obtained using the OSA) and Fig. 8 shows the measurements using the proposed demodulation method (2 seconds sampling interval). Although a 2 second sampling interval was chosen, we estimate the model would take 0.0350 ± 0.0002 seconds to make an estimation using a dropout ensemble of 10 rounds at an Intel i7 12700H laptop with 32 GB RAM, running TensorFlow via Keras with CUDA on a 6 GB Nvidia RTX 3060. Which is faster than the 50 minutes sampling rate of [32] and the 15 minutes of [31], despite being slower than the 0.01 seconds of [33].

During calibration we observed the resonant dip shifted towards lower wavelengths and the resonance dip reduced attenuation. Although the proposed system does not estimate the dip attenuation, one can clearly see the sensor's blue shift in Fig. 8. Hence, our proposal was able to capture the sample variation and the transitory states regarding sample change. The estimated resonant wavelength for each step can be seen in Table II.

The blue shift regarding the water sample was calculated and applied to the calibration curve, to estimate the sample refractive index. Considering the resonant wavelength values

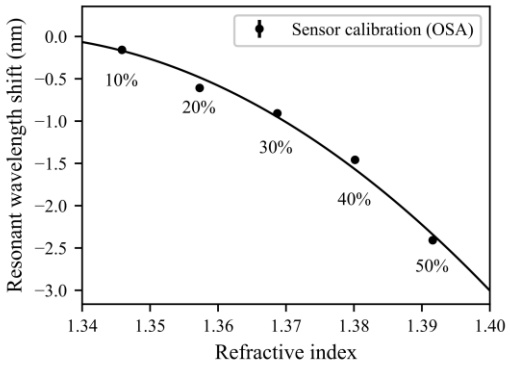

Fig. 7. LPFG sensor calibration.

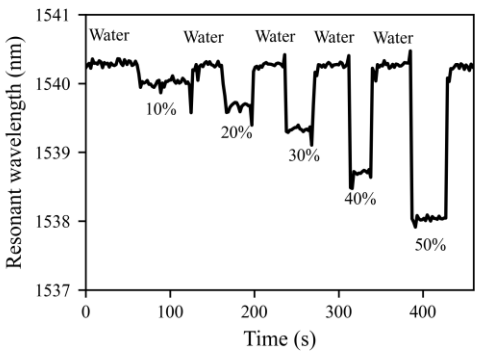

Fig. 8. LPFG demodulation by the proposed method.

TABLE II. PROPOSED MODEL RI SENSOR READINGS

Sample	Resonant wavelength (nm)	Estimated RI	Target RI
10%	1540.01 ± 0.02	1.350 ± 0.001	1.34751 ± 0.00018
20%	1539.67 ± 0.03	1.360 ± 0.001	1.35938 ± 0.00022
30%	1539.34 ± 0.01	1.3683 ± 0.0005	1.36740 ± 0.00026
40%	1538.71 ± 0.01	1.3799 ± 0.0003	1.38103 ± 0.00032
50%	1540.25 ± 0.01	1.3898 ± 0.0004	1.3928 ± 0.0004

shown in Table II we estimated the RI also shown in this table. The estimations were compared to the target RI and we estimated the residual mean and standard deviation as -0.0001 RIU and 0.001 RIU, which is 0.072% of target RI. Note, however, that most error occurs for lower RI, where the sensitivity is smaller. This indicates that the error might not be due to wrong resonant wavelength estimation, but to poor sensor response. Indeed, wrong resonant wavelength estimation would introduce more RI error at the higher sensitivity part of the sensor response because little wavelength difference would imply great RI difference.

Finally, to evaluate FBGs-LPFG decoupling, the LPFG sensor was kept in water while the FBGs at 1538.730 nm, 1544.230 nm, and 1550.039 nm (at the beginning of this experiemnt) were shifted up to 800 pm. The mean value for the LPFG sensor was 1540.33 nm with an standard deviation of 0.24 nm, as expected for the water sample. To evaluate if the FBG shift disturbed the LPFG position, the correlation coefficient between FBGs position and the LPFG position was calculated. The correlation between FBGs and LPFG wavelengths were: 0.11, -0.064, 0.028 for the FBGs at 1538 nm, 1544 nm, and 1550 nm, respectivelly, demonstrating that the proposed method can identify the LPFG position despite FBG shifting, thus forming a robust sensor network.

V. CONCLUSIONS

Long-period fiber gratings (LPFGs) possess unique metrological properties and a wide range of applications. However, their limited adoption stems from challenges in multiplexing and interrogation, limiting the potential for in-field applications.

This work proposes a novel approach to address these limitations and unlock the full potential of LPFGs. We combine machine learning with FBG sensor arrays, enabling efficient LPFG use in a commercially available sensing solution. By employing a self-attention-based model trained with synthetic data, the system overcomes the need for a vast collection of real-world measurements. The self-attention mechanism itself acts as a powerful filter, focusing on relevant spectral features crucial for LPFG demodulation.

The results are promising. Our model demonstrably outperforms traditional methods when evaluated with real LPFG spectra. This signifies significant progress towards simplified interrogation techniques, a major hurdle for LPFG adoption. The results showed good generalization capability concerning synthetic training and transfer learning to real measurements. With a high number of available training data, new models such as convolutional networks, transformers and other robust machine learning technologies to further improve the LPFG interrogation paradigm.

Table III shows a comparison between LPFG interrogation approaches. It shows whether the method is LPFG-agnostic (if LPFG spectra must be known, or the system recalibrated for each LPFG sensor), the resolution, number of sensors, and acquisition time. Note that the proposed method provides resolution compared to results found in the literature, as fast as the fastest approach, while significantly expanding the number of sensing heads. This improves significantly the overall cost-effectiveness of the optical sensing systems and allows the use of LPFGs alongside well stablished FBG sensors.

These advancements pave the way for broader LPFG utilization in various sensing applications. By simplifying interrogation and leveraging the power of machine learning, this work opens doors to a future where LPFGs can truly realize

TABLE III. LPFG INTERROGATION COMPARISON

Ref.	LPFG agnostic	Resolution	Measurement range	Number of sensing heads	Acquisition time	Number of channels	Estimation method
[35]	No	5 με/0.5 °C	-	2	-	2	Linear fitting
[34]	No	1.75 pm	1537-1547 nm	1	-	1 (modulated)	Harmonics + linear fitting
[30]	Yes	0.07 nm	1540-1562 nm	1	-	32	Gaussian fitting
[29]	Yes	1 pm	25 nm	1	-	32 (modulated)	Curve fitting
[37]	Yes	2.85 nm	1510-1585 nm	1	-	13	Perceptron network
[38]	Yes	0.481 nm	1510-1585 nm	1	-	13	Fuzzy system
[31]	Yes	1.12 nm	1530-1570 nm	1	15 min.	3 (modulated)	Lorentzian fitting
[32]	Yes	0.4 nm	1298-1308 nm	1	50 min.	1 (modulated)	Gaussian fitting
[33]	Yes	5×10^{-4} RIU / 0.8 °C	1350-1650 nm	1	0.01 sec.	1 (modulated)	Wiener deconvolution
Proposed method	Yes	0.687 nm / 1×10^{-3} RIU	1515-1585 nm	14	0.0350 sec.	13 (arbitrary position)	Self-attention network

their full potential in the field of sensor technology.

REFERENCES

[1] L. H. Silva, P. Santos, L. C. C. Coelho, P. Jorge, and J. M. Baptista, "Development of a Long Period Fiber Grating Interrogation System Using a Multimode Laser Diode," *Sensors*, vol. 21, no. 3, p. 749, Jan. 2021, doi: 10.3390/s21030749.

[2] E. A. Souza, L. C. Macedo, A. Frizera, C. Marques, and A. Leal-Junior, "Fiber Bragg Grating Array for Shape Reconstruction in Structural Elements," *Sensors*, vol. 22, no. 17, p. 6545, Aug. 2022, doi: 10.3390/s22176545.

[3] W. Gao, J. Liu, H. Guo, X. Jiang, S. Sun, and H. Yu, "Multi-Wavelength Ultra-Weak Fiber Bragg Grating Arrays for Long-Distance Quasi-Distributed Sensing," *Photonic Sensors*, vol. 12, no. 2, pp. 185–195, Jun. 2022, doi: 10.1007/s13320-021-0635-4.

[4] T. Allsop, T. Earthrowl, R. Reeves, D. J. Webb, and I. Bennion, "The interrogation and multiplexing of long period grating curvature sensors using a Bragg grating based, derivative spectroscopy technique," *Meas Sci Technol*, vol. 15, no. 1, pp. 44–48, Jan. 2004, doi: 10.1088/0957-0233/15/1/006.

[5] I. Torres-Gómez, A. Martínez-Rios, G. Anzueto-Sánchez, Daniel. E. Ceballos-Herrera, and G. Salceda-Delgado, "Transverse Load and Temperature Sensing Using Multiplexed Long-Period Fiber Gratings," *Photonics*, vol. 8, no. 1, p. 1, Dec. 2020, doi: 10.3390/photonics8010001.

[6] C. Colaco, P. Caldas, I. Del Villar, R. Chibante, and G. Rego, "Arc-Induced Long-Period Fiber Gratings in the Dispersion Turning Points," *Journal of Lightwave Technology*, vol. 34, no. 19, pp. 4584–4590, Oct. 2016, doi: 10.1109/JLT.2016.2540678.

[7] F. de S. Delgado and A. B. dos Santos, "Reduction of intrinsic polarization dependence in arc-induced long-period fiber gratings," *Optical Engineering*, vol. 57, no. 06, p. 1, Jun. 2018, doi: 10.1117/1.OE.57.6.067105.

[8] F. Esposito, R. Ranjan, S. Campopiano, and A. Iadicicco, "Experimental Study of the Refractive Index Sensitivity in Arc-induced Long Period Gratings," *IEEE Photonics J*, vol. 9, no. 1, pp. 1–10, Feb. 2017, doi: 10.1109/JPHOT.2016.2634784.

[9] Q. Ling, Z. Gu, W. Wu, and B. Pang, "Simultaneous SRI and temperature measurement of FM-LPFG written by CO2 laser," *Optical Fiber Technology*, vol. 58, p. 102264, Sep. 2020, doi: 10.1016/j.yofte.2020.102264.

[10] X. Lan *et al.*, "Turn-around point long-period fiber grating fabricated by CO2 laser for refractive index sensing," *Sens Actuators B Chem*, vol. 177, pp. 1149–1155, Feb. 2013, doi: 10.1016/j.snb.2012.12.006.

[11] B. Li, L. Jiang, S. Wang, H.-L. Tsai, and H. Xiao, "Femtosecond laser fabrication of long period fiber gratings and applications in refractive index sensing," *Opt Laser Technol*, vol. 43, no. 8, pp. 1420–1423, Nov. 2011, doi: 10.1016/j.optlastec.2011.04.011.

[12] Y.-J. Rao, "Novel mechanical fiber optic sensors based on long-period fiber gratings written by high-frequency CO 2 laser pulses," Y.-J. Rao, J. D. C. Jones, H. Naruse, and R. I. Chen, Eds., Sep. 2002, p. 43. doi: 10.1117/12.482004.

[13] Q. Hu *et al.*, "Raman suppression in 5 kW fiber amplifier using long period fiber grating fabricated by CO2 laser," *Opt Laser Technol*, vol. 145, p. 107484, Jan. 2022, doi: 10.1016/j.optlastec.2021.107484.

[14] N. Lee, J. Song, and J. Park, "Mechanically induced long-period fiber grating array sensor," *Microw Opt Technol Lett*, vol. 53, no. 10, pp. 2295–2298, Oct. 2011, doi: 10.1002/mop.26289.

[15] S. Zahra, P. Di Palma, E. De Vita, F. Esposito, A. Iadicicco, and S. Campopiano, "Investigation of mechanically induced long period grating by 3-D printed periodic grooved plates," *Opt Laser Technol*, vol. 167, p. 109752, Dec. 2023, doi: 10.1016/j.optlastec.2023.109752.

[16] Xuewen Shu *et al.*, "Sensitivity characteristics of long-period fiber gratings," *Journal of Lightwave Technology*, vol. 20, no. 2, pp. 255–266, 2002, doi: 10.1109/50.983240.

[17] M. Peng *et al.*, "Femtosecond laser direct writing of long period fiber grating sensor with high refractive index sensitivity," *Optical Fiber Technology*, vol. 81, p. 103511, Dec. 2023, doi: 10.1016/j.yofte.2023.103511.

[18] L. Coelho, D. Viegas, J. L. Santos, and J. M. M. M. de Almeida, "Detection of Extra Virgin Olive Oil Thermal Deterioration Using a Long Period Fibre Grating Sensor Coated with Titanium Dioxide," *Food Bioproc Tech*, vol. 8, no. 6, pp. 1211–1217, Jun. 2015, doi: 10.1007/s11947-015-1489-9.

[19] R. L. Faraco Filho, F. Oliveira Barino, J. Calderano, Í. F. Valle Alvarenga, D. Campos, and A. B. dos Santos, "In-fiber Mach–Zehnder interferometer as a promising tool for optical nose and odor prediction during the fermentation process," *Opt Lett*, vol. 48, no. 15, p. 3905, Aug. 2023, doi: 10.1364/OL.486742.

[20] M. Delgado-Pinar *et al.*, "Oligonucleotide-Hybridization Fiber-Optic Biosensor Using a Narrow Bandwidth Long Period Grating," *IEEE Sens J*, vol. 17, no. 17, pp. 5503–5509, Sep. 2017, doi: 10.1109/JSEN.2017.2723759.

[21] F. Esposito *et al.*, "Label-free detection of vitamin D by optical biosensing based on long period fiber grating," *Sens Actuators B Chem*, vol. 347, p. 130637, Nov. 2021, doi: 10.1016/j.snb.2021.130637.

[22] S. He *et al.*, "Bacterial Detection and Differentiation of Staphylococcus aureus and Escherichia coli Utilizing Long-Period Fiber Gratings Functionalized with Nanoporous Coated Structures," *Coatings*, vol. 13, no. 4, p. 778, Apr. 2023, doi: 10.3390/coatings13040778.

[23] X. Kang *et al.*, "A label-free biosensor for pepsin detection based on graphene oxide functionalized micro-tapered long period fiber grating," *Sensors and Actuators Reports*, vol. 5, p. 100139, Jun. 2023, doi: 10.1016/j.snr.2023.100139.

[24] R. Wang, Z. Ren, D. Kong, B. Hu, and Z. He, "Highly sensitive label-free biosensor based on graphene-oxide functionalized micro-tapered long period fiber grating," *Opt Mater (Amst)*, vol. 109, p. 110253, Nov. 2020, doi: 10.1016/j.optmat.2020.110253.

[25] B. Xu, J. Huang, L. Ding, and J. Cai, "Graphene oxide-functionalized long period fiber grating for ultrafast label-free glucose biosensor," *Materials Science and Engineering: C*, vol. 107, p. 110329, Feb. 2020, doi: 10.1016/j.msec.2019.110329.

[26] K. Ren *et al.*, "Polyvinyl Alcohol Nanofibers Wrapped Microtapered Long-Period Fiber Grating for High-Linearity Humidity and Temperature Sensing," *IEEE Sens J*, vol. 24, no. 5, pp. 6279–6285, Mar. 2024, doi: 10.1109/JSEN.2024.3354055.

[27] G. Zhou, F. Tang, G. Li, Z. Lin, and H.-N. Li, "Long-Period Grating Fiber Optic Sensors Coated With Gold Film and Pulse-Electroplated Iron–Carbon Layer for Reinforcing Steel Corrosion Monitoring," *IEEE Trans Instrum Meas*, vol. 72, pp. 1–11, 2023, doi: 10.1109/TIM.2023.3284925.

[28] Y. Zhuo and G. Chen, "Recent development of Fe-C coated long-period fiber gratings, corrosion sensors," in *Optical Waveguide and Laser Sensors II*, G. A. Sanders, R. A. Lieberman, and I. Udd Scheel, Eds., SPIE, Jun. 2023, p. 1. doi: 10.1117/12.2665270.

[29] H. Guo, G. Xiao, N. Mrad, and J. Yao, "Interrogation of a long-period grating sensor by a thermally tunable arrayed waveguide grating," *IEEE Photonics Technology Letters*, vol. 20, no. 21, pp. 1790–1792, 2008.

[30] H. Guo, G. Xiao, and J. Yao, "Interrogation of a Long Period Grating Fiber Sensor With an Arrayed-Waveguide-Grating-Based Demultiplexer Through Curve Fitting," *IEEE Sens J*, vol. 8, no. 11, pp. 1771–1775, Nov. 2008, doi: 10.1109/JSEN.2008.2004472.

[31] P. S. S. dos Santos, P. A. S. Jorge, J. de Almeida, and L. Coelho, "Low-Cost Interrogation System for Long-Period Fiber Gratings Applied to Remote Sensing," *Sensors*, vol. 19, no. 7, p. 1500, Mar. 2019, doi: 10.3390/s19071500.

[32] L. H. Silva, P. Santos, L. C. C. Coelho, P. Jorge, and J. M. Baptista, "Development of a Long Period Fiber Grating Interrogation System Using a Multimode Laser Diode," *Sensors*, vol. 21, no. 3, p. 749, Jan. 2021, doi: 10.3390/s21030749.

[33] J. C. C. Araújo, P. S. S. dos Santos, B. Dias, J. M. M. M. de Almeida, and L. C. C. Coelho, "Low-Cost Wideband Interrogation System for Fiber Optic Sensors," *IEEE Sens J*, vol. 23, no. 13, pp. 14315–14322, Jul. 2023, doi: 10.1109/JSEN.2023.3272368.

[34] G. Sampaio, F. O. Barino, and A. B. dos Santos, "Long-period fiber grating sensor interrogation with single strain modulated FBG and harmonic analysis," *Optical Fiber Technology*, vol. 71, p. 102940, Jul. 2022, doi: 10.1016/j.yofte.2022.102940.

[35] H. J. Patrick, G. M. Williams, A. D. Kersey, J. R. Pedrazzani, and A. M. Vengsarkar, "Hybrid fiber Bragg grating/long period fiber

grating sensor for strain/temperature discrimination," *IEEE Photonics Technology Letters*, vol. 8, no. 9, pp. 1223–1225, Sep. 1996, doi: 10.1109/68.531843.

[36] R. Yan, S. Wang, Q. Jiao, and L. Bian, "Computational spectrometer based on local feature-weighted spectral reconstruction," *Opt Express*, vol. 31, no. 9, p. 14240, Apr. 2023, doi: 10.1364/OE.488854.

[37] F. O. Barino, A. B. d. Santos, and A. B. dos Santos, "LPG Interrogator Based on FBG Array and Artificial Neural Network," *IEEE Sens J*, vol. 20, no. 23, pp. 14187–14194, Dec. 2020, doi: 10.1109/JSEN.2020.3007957.

[38] F. O. Barino, E. P. De Aguiar, L. De Mello Honório, V. N. H. Silva, A. P. López-Barbero, and A. B. Dos Santos, "A Fuzzy Approach to LPFG-Based Optical Sensor Processing and Interrogation," *IEEE Trans Instrum Meas*, vol. 71, 2022, doi: 10.1109/TIM.2022.3216390.

[39] C. Li, J. Tang, C. Cheng, L. Cai, and M. Yang, "FBG Arrays for Quasi-Distributed Sensing: A Review," *Photonic Sensors*, vol. 11, no. 1, pp. 91–108, Mar. 2021, doi: 10.1007/s13320-021-0615-8.

[40] Y. Qi *et al.*, "Research on temperature and humidity sensing characteristics of cascaded LPFG-FBG," *Optik (Stuttg)*, vol. 188, pp. 19–26, Jul. 2019, doi: 10.1016/j.ijleo.2019.05.043.

[41] T. Zhang, Z. Tong, and C. Yang, "Real-time monitoring and decoupling of multi parameters in vascular intervention using a cascaded LPFG-FBG sensor," *Sens Actuators A Phys*, vol. 359, p. 114463, Sep. 2023, doi: 10.1016/j.sna.2023.114463.

[42] Z. S. Alshaikhli, "Structural health monitoring of underground pipelines using polyimide coated LPFG-FBG-LPFG: simultaneous modeling of temperature and pressure effects," *Journal of Optics*, vol. 53, no. 2, pp. 1492–1498, Apr. 2024, doi: 10.1007/s12596-023-01314-7.

[43] C. Wei *et al.*, "Deep Learning Enhanced Fiber-Optic Fabry–Perot Sensor Demodulation With Sparse Sampling Points Using GAF Algorithm," *IEEE Sens J*, vol. 24, no. 16, pp. 26845–26852, Aug. 2024, doi: 10.1109/JSEN.2024.3416994.

[44] Z. Yue, D. Zheng, X. Zou, C. Xie, and Y. Peng, "Large Dynamic Range Interrogation Technique for Fiber-Optic Interferometric Sensor Based on AWG and Deep Learning Algorithm," *IEEE Sens J*, vol. 24, no. 1, pp. 278–286, Jan. 2024, doi: 10.1109/JSEN.2023.3329299.

[45] S. Ren *et al.*, "Rethink Training: Synthetic Data Powers Efficient Fiber-Optics Sensor Demodulation Neural Networks," *IEEE Sens J*, vol. 24, no. 19, pp. 31408–31416, Oct. 2024, doi: 10.1109/JSEN.2024.3441239.

[46] F. Barino, "lpfg_demodulation_supplementary," 2025. doi: 10.5281/zenodo.15024268.

[47] A. Vaswani *et al.*, "Attention Is All You Need," in *Advances in Neural Information Processing Systems 30* , 2017.

[48] Z. Niu, G. Zhong, and H. Yu, "A review on the attention mechanism of deep learning," *Neurocomputing*, vol. 452, pp. 48–62, Sep. 2021, doi: 10.1016/j.neucom.2021.03.091.

[49] R. L. Faraco *et al.*, "Hydroelectric Plant Safety: Real-Time Monitoring Utilizing Fiber-Optic Sensors," *Sensors 2024, Vol. 24, Page 4601*, vol. 24, no. 14, p. 4601, Jul. 2024, doi: 10.3390/S24144601.

[50] C. J. Hoel, K. Wolff, and L. Laine, "Ensemble Quantile Networks: Uncertainty-Aware Reinforcement Learning With Applications in Autonomous Driving," *IEEE Transactions on Intelligent Transportation Systems*, vol. 24, no. 6, pp. 6030–6041, Jun. 2023, doi: 10.1109/TITS.2023.3251376.

[51] Y. Gal and Z. Ghahramani, "Dropout as a Bayesian Approximation: Representing Model Uncertainty in Deep Learning," in *Proceedings of the 33rd International Conference on International Conference on Machine Learning - Volume 48*, 2016, pp. 1050–1059.

[52] E. Hüllermeier and W. Waegeman, "Aleatoric and epistemic uncertainty in machine learning: an introduction to concepts and methods," *Mach Learn*, vol. 110, no. 3, pp. 457–506, Mar. 2021, doi: 10.1007/S10994-021-05946-3/FIGURES/17.

Felipe Barino (Member, IEEE) was born in 1996 in Juiz de Fora, Brazil, is an engineer and researcher in the field of instrumentation and electronics.

He earned his B.S., M.Sc., and Ph.D. degrees from the Federal University of Juiz de Fora (UFJF) in 2019, 2021, and 2025, respectively. From his undergraduate years, Felipe has been an active researcher at the Laboratório de Instrumentação e Telemetria (LITel). His research endeavors primarily focus on instrumentation, metrology, optical fiber sensors, sensor packaging, machine learning, and transfer learning.

Alexandre Bessa dos Santos (Member, IEEE) was born in Juiz de Fora, Brazil, in 1975. He received the M.Sc. and Ph.D. degrees in electrical engineering from Pontifical Catholic University (PUC), Rio de Janeiro, Brazil, in 2001 and 2005, respectively. Since 2010, he has been an Associate Professor with the Department of Circuits, Federal University of Juiz de Fora (UFJF), Juiz de Fora. His research interests include applied electromagnetism, optical sensors, computational methods, instrumentation, and metrology.